IEEE Robotics and Automation Letters (RA-L) paper, presented at ICRA 2026, Vienna, Austria. Cite as RA-L paper.

A Real-Time 6-DoF Posture Estimation Method for High-Speed 6-Axis Industrial Manipulator Control Using a 2D Laser Profiler

Tao Chen, Pei-Chun Lin

***Abstract*—6-DoF posture estimation is a critical technique in robotics. However, a significant gap exists between the two primary approaches—camera-based methods and laser tracker systems—in terms of cost and performance. To bridge this gap, this work proposes a method to calculate the 6-DoF posture of a manipulator's end-effector using the 2D profile of a custom-designed metallic gauge. The core principle relies on a one-to-one correspondence between the measured profile and the manipulator's posture. A mathematical model was developed to derive a closed-form solution, which is further refined via maximum likelihood estimation to enhance robustness and accuracy. Simulation studies assessed the influence of geometric parameters on estimation accuracy and noise robustness. Real-world experiments demonstrated that the refined solution significantly outperforms the closed-form solution alone. Furthermore, a speed benchmark against a camera-based system highlighted the proposed method's advantage in operating frequency. Finally, the method was successfully integrated into a real-time position control task for a 6-axis industrial manipulator, verifying its practical applicability in real-time robotic control.**

***Index Terms*—Range Sensing, Localization, Sensor-based Control, Manipulation**

I. Introduction

POSTURE estimation with six degrees of freedom posture estimation, comprising three translational and three rotational components, is a critical capability in robotics and related fields such as autonomous driving [1] and augmented/virtual reality (AR/VR) [2]. In autonomous vehicles, six-degree-of-freedom (6-DoF) estimation enables accurate navigation and obstacle avoidance, facilitating safe operation. Similarly, in AR/VR systems, precise tracking of user motion and equipment is essential for seamless virtual-physical integration. For industrial robotics, manipulators rely heavily on accurate 6-DoF feedback for kinematic calibration, precise navigation, stability maintenance, and effective interaction with complex environments [3]. Robust, high-frequency posture information is thus fundamental for advanced tasks, including dynamic trajectory tracking, adaptive control, and environment-aware manipulation.

While camera-based systems are widely used for applications like object detection, self-relocalization [4], and self-calibration [5] due to the intuitive nature of image data, they face limitations in high-frequency control. The large data volume of images results in significant transmission and processing latencies, restricting their operating frequency. In contrast, laser tracker systems offer high-speed, high-accuracy 6-DoF measurements and are suitable for real-time control of high-dynamic systems. However, their high cost and limited accessibility prevent widespread deployment.

Industrial manipulators often execute dynamic trajectories with rapid motion changes, inducing unexpected behaviors due to low structural stiffness. Real-time posture feedback is therefore critical for stabilization. To bridge the gap between expensive laser trackers and lower-frequency camera systems, this paper presents a real-time 6-DoF posture estimation method using a 2D laser profiler and a custom-designed metallic gauge. 2D laser profilers (laser line scanners) acquire cross-sectional depth measurements via triangulation [6]. Their high accuracy, fast sampling, and robustness to lighting variations have enabled applications in inspection [7], welding monitoring [8], object posture estimation [9], and kinematic calibration [10], [11]. Unlike cameras [12], [13], however, laser profilers provide limited spatial context, complicating direct 6-DoF estimation. Existing solutions typically address relative 6-DoF calibration between multiple sensors, such as multiple profilers [14] or profilers with external sensors [15]. These systems commonly rely on external tracking systems or markers, increasing complexity and cost.

To address the need for direct, markerless, real-time 6-DoF estimation under dynamic conditions, we propose a methodology utilizing profile data from a custom metallic gauge scanned by a single 2D laser profiler. We develop a closed-form solution augmented with maximum likelihood estimation (MLE) refinement, achieving computation times under 1 ms and stable operation at a 12 ms control period (accounting for transmission delays). By exploiting geometric correspondences between the gauge's corner points and the measured profile, our approach provides precise, efficient state estimation. Extensive simulations and experiments demonstrate that this method offers a cost-effective, high-frequency alternative that bridges the gap between costly laser trackers and traditional low-frequency vision systems.

To our knowledge, this is the first work to derive a closed-form solution for 6-DoF posture estimation using a single laser profiler. The proposed approach offers reduced data latency and faster data processing speed compared to camera-based systems. The key contributions of this letter are:

1) Derivation of a closed-form solution for 6-DoF posture

Manuscript received: September, 18, 2025; Revised November, 30, 2025; Accepted December, 28, 2025.

This paper was recommended for publication by Editor Pascal Vasseur. Name upon evaluation of the Associate Editor and Reviewers' comments. National Science and Technology Council (NSTC), Taiwan, under Contract 112-2634-F-007-002 and 113-2634-F-007-002-.

The authors are with the Department of Mechanical Engineering, National Taiwan University, Taiwan d10522001@ntu.edu.tw; peichunlin@ntu.edu.tw

Digital Object Identifier (DOI): see top of this page.

IEEE Robotics and Automation Letters (RA-L) paper, presented at ICRA 2026, Vienna, Austria. Cite as RA-L paper.

estimation using a laser profiler, refined via maximum likelihood estimation.
2) Analysis and design guidelines for a custom gauge that balances estimation quality with fabrication complexity.
3) Benchmark validation demonstrating superior speed compared to camera-based methods.
4) Verification of practicality through real-time closed-loop position control of a six-axis industrial manipulator.

II. NOVEL LASER PROFILING METHODOLOGY

A. System Architecture

Fig. 1(a) illustrates the system architecture of the proposed real-time 6-DoF posture estimation method for a 6-axis industrial manipulator. The system comprises a 2D laser profiler mounted on the manipulator's flange (hereafter referred to as the end-effector), a manipulator controller, a microcontroller, a laser profiler controller, a custom-designed gauge, and a real-time processing unit.

In each control cycle, the manipulator controller transmits a digital signal to the microcontroller. The microcontroller subsequently generates two digital trigger signals for the laser profiler controller, initiating a scan of the gauge by the 2D laser profiler. The acquired profile data is transmitted to the laser profiler controller via a physical cable and then forwarded to the real-time processing unit over TCP. The processing unit estimates the end-effector's 6-DoF posture and computes a compensation command to rectify deviations between the reference and estimated postures. This updated command is sent to the manipulator controller via TCP using the manufacturer's robot interface.

The microcontroller plays a critical role in ensuring real-time performance. Because the laser profiler controller releases data only upon external triggering, the microcontroller's dual-signal sequence ensures the profile data reaches the processing unit within the current control cycle. Without this synchronization mechanism, the system would suffer from a one-period delay, degrading real-time feedback quality and potentially destabilizing the closed-loop control.

B. Experimental Hardware Setup

Fig. 1(b) depicts the complete hardware setup for the proposed 6-DoF posture estimation system. All experiments were conducted using a Yaskawa GP12 6-axis industrial manipulator, characterized by a 12 kg payload, a horizontal reach of 1440 mm, a vertical reach of 2511 mm, and a position repeatability of ± 0.02 mm. A Keyence LJ-X8400 2D laser profiler, controlled by an LJ-X8000A controller, was mounted directly on the manipulator's end-effector. This profiler offers a maximum acquisition rate of 1 kHz and a trapezoidal measurement range with depths from 285 mm to 600 mm and widths from 163 mm to 320 mm. Each scan generates 3200 profile points at 0.075 mm intervals, achieving a repeatability of 10 μm in the x-axis and 5 μm in the z-axis. The real-time processing unit consists of a workstation running Linux, equipped with an Intel i9-12900KF CPU, 32 GB RAM, and an NVIDIA RTX 3070 GPU. An Arduino Nano microcontroller handles signal conversion and triggering, satisfying all timing

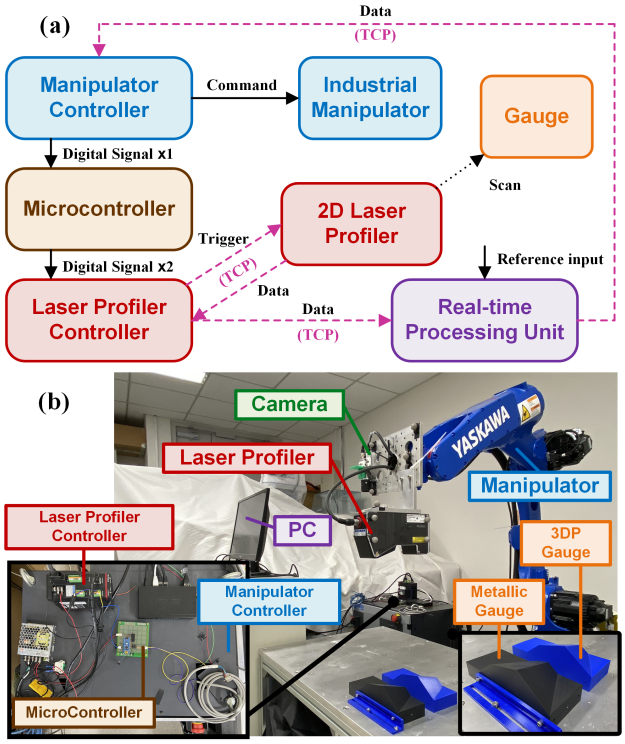

Fig. 1. (a) System architecture and (b) experimental setup of the proposed 6-DoF posture estimation method. Components include the the 6-axis industrial manipulator, manipulator controller, 2D laser profiler, laser profiler controller, microcontroller, custom gauges (metallic and 3DP), and the real-time processing unit.

and I/O requirements. Profile data is continuously acquired and transmitted to the workstation for posture estimation at a 12 ms period via the MotoPlus SDK robot interface.

For benchmarking, a camera-based system was established, comprising a Basler AC2500-14gc industrial camera (2590×1942 resolution) and an 8×11 chessboard target with 20 mm squares. Image acquisition was managed by the Pylon SDK, with posture estimation performed on the workstation using the OpenCV library.

The custom metallic gauge features a matte surface finish to induce diffuse reflection, optimizing compatibility with the laser profiler. Additionally, a 3D-printed gauge with identical geometry was fabricated using an UltiMaker S5 via fused deposition modeling for the benchmarking experiments detailed in Section IV-A.

C. Mathematical Model of 6-DoF Posture Estimation Using 2D Profile Data

The fundamental principle underlying 6-DoF posture estimation from the gauge's 2D profile relies on geometric constraints imposed by the gauge design. The gauge comprises multiple non-parallel, consecutive planar surfaces that produce a polyline in the measured 2D profile. Each plane generates a line segment in the profile, while the intersections of adjacent planes—referred to as ridges—correspond to the polyline's corner points. The methodology exploits a one-to-one correspondence between the measured profile and the manipulator end-effector's posture, analogous to camera-based 6-DoF

IEEE Robotics and Automation Letters (RA-L) paper, presented at ICRA 2026, Vienna, Austria. Cite as RA-L paper.

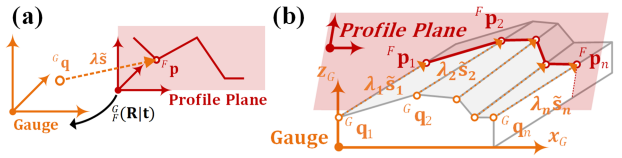

Fig. 2. The illustration of (a) the notations used in the proposed 6-DoF posture estimation method and (b) the profile that has n corner points.

estimation using chessboard patterns, where image features uniquely determine camera pose. To facilitate derivation of the mathematical model, the relevant notation is first introduced and illustrated in Fig. 2.

The gauge coordinate system is denoted by $\mathbf{G}$, while the laser profiler coordinate system is denoted by $\mathbf{F}$, with its x-z plane coincident with the laser profiler's emitted laser plane. Arbitrary 3D points $\mathbf{p}$ in space can be expressed in the gauge coordinate system and the laser profiler coordinate system as ${}^{G}\mathbf{p} = [{}^{G}p_x \;\; {}^{G}p_y \;\; {}^{G}p_z]^\top$ and ${}^{F}\mathbf{p} = [{}^{F}p_x \;\; {}^{F}p_y \;\; {}^{F}p_z]^\top$, respectively. Augmented vector representation is denoted by a tilde symbol: ${}^{G}\tilde{\mathbf{p}} = [{}^{G}p_x \;\; {}^{G}p_y \;\; {}^{G}p_z \;\; 1]^\top$ and ${}^{F}\tilde{\mathbf{p}} = [{}^{F}p_x \;\; {}^{F}p_y \;\; {}^{F}p_z \;\; 1]^\top$. The relationship between a 3D point represented in $\mathbf{G}$ and $\mathbf{F}$ is given by

$$ {}^{G}\mathbf{p} = {}^{G}_{F}(\mathbf{R}|\mathbf{t})\, {}^{F}\tilde{\mathbf{p}} \tag{1} $$

where $\mathbf{R} \in SO(3)$ and $\mathbf{t} \in \mathbb{R}^3$ denote the rotation matrix and translation vector, respectively, that transform coordinates from the laser profiler frame to the gauge frame. The posture estimation involves determining the transformation ${}^{G}_{F}(\mathbf{R}|\mathbf{t})$, which describes the laser profiler's pose relative to the gauge, based on known point correspondences between ${}^{G}\tilde{\mathbf{p}}$ and ${}^{F}\tilde{\mathbf{p}}$.

The solution is formulated based on the Direct Linear Transformation (DLT) algorithm, which is widely applied to Perspective-n-Point problems in computer vision [16]. The derivation begins by considering a corner point ${}^{F}\mathbf{p}$ on the 2D profile, which lies on the intersection line of two adjacent gauge planes, denoted as $\mathbf{L}$. The corresponding position in the gauge frame is denoted by ${}^{G}\mathbf{p}$. Since the gauge geometry is known a priori, the line $\mathbf{L}$ on which ${}^{G}\mathbf{p}$ lies can be parameterized by a direction vector $\tilde{\mathbf{s}} = [u \; 1 \; w]^\top$ and a known point ${}^{G}\mathbf{q} = [{}^{G}q_x \;\; {}^{G}q_y \;\; {}^{G}q_z]^\top$ on the line:

$$ \mathbf{L} : {}^{G}\mathbf{q} + \lambda\tilde{\mathbf{s}} = \begin{bmatrix} {}^{G}q_x \\ {}^{G}q_y \\ {}^{G}q_z \end{bmatrix} + \lambda \begin{bmatrix} u \\ 1 \\ w \end{bmatrix} \tag{2} $$

where λ is a scalar parameter. The direction vector $\tilde{\mathbf{s}}$ employs the tilde notation to indicate augmentation from the 2D vector $\mathbf{s} = [u \; w]^\top$ by setting the second component to unity. Since ${}^{G}\mathbf{p}$ lies on $\mathbf{L}$, it can be expressed as:

$$ {}^{G}\mathbf{p} = \begin{bmatrix} {}^{G}q_x \\ {}^{G}q_y \\ {}^{G}q_z \end{bmatrix} + \hat{\lambda} \begin{bmatrix} u \\ 1 \\ w \end{bmatrix} \tag{3} $$

where $\hat{\lambda}$ is the scalar parameter that locates ${}^{G}\mathbf{p}$ along $\mathbf{L}$. Substituting (3) into (1), where $\mathbf{r}_j$ denotes the j^{th} column of $\mathbf{R}$, yields:

$$ \begin{bmatrix} {}^{G}q_x \\ {}^{G}q_y \\ {}^{G}q_z \end{bmatrix} + \hat{\lambda} \begin{bmatrix} u \\ 1 \\ w \end{bmatrix} = \begin{bmatrix} \mathbf{r}_1 & \mathbf{r}_2 & \mathbf{r}_3 & \mathbf{t} \end{bmatrix} {}^{F}\tilde{\mathbf{p}} \tag{4} $$

Given that ${}^{F}\tilde{\mathbf{p}}$ is expressed in the laser profiler coordinate system, its y-component ${}^{F}p_y$ must be zero, since the profile lies entirely within the x-z plane. Setting ${}^{F}p_y = 0$ in (4) eliminates the $\mathbf{r}_2$ contribution, resulting in:

$$ \begin{bmatrix} {}^{G}q_x \\ {}^{G}q_y \\ {}^{G}q_z \end{bmatrix} + \hat{\lambda} \begin{bmatrix} u \\ 1 \\ w \end{bmatrix} = \begin{bmatrix} \mathbf{r}_1 & \mathbf{r}_3 & \mathbf{t} \end{bmatrix} \begin{bmatrix} {}^{F}p_x \\ {}^{F}p_z \\ 1 \end{bmatrix} \tag{5} $$

Eq. (5) thus establishes the fundamental relationship between the profile corner point expressed in both the gauge and laser profiler coordinate systems. Redefining $[\mathbf{r}_1 \; \mathbf{r}_3 \; \mathbf{t}]$ as $\mathbf{M}$, and reusing the notation ${}^{F}\tilde{\mathbf{p}}$ to denote $[{}^{F}p_x \;\; {}^{F}p_z \;\; 1]^\top$ for brevity, yields:

$$ \begin{bmatrix} {}^{G}q_x \\ {}^{G}q_y \\ {}^{G}q_z \end{bmatrix} + \hat{\lambda} \begin{bmatrix} u \\ 1 \\ w \end{bmatrix} = \mathbf{M}\, {}^{F}\tilde{\mathbf{p}} \tag{6} $$

which provides a concise representation of the corner point correspondence between both coordinate frames.

Denoting the k^{th} row of $\mathbf{M}$ by $\mathbf{m}_k^\top$, expansion of (6) yields constraints along each axis of the gauge coordinate system:

$$ \begin{cases} {}^{G}q_x + \hat{\lambda}u = \mathbf{m}_1^\top \cdot {}^{F}\tilde{\mathbf{p}} \\ {}^{G}q_y + \hat{\lambda} = \mathbf{m}_2^\top \cdot {}^{F}\tilde{\mathbf{p}} \\ {}^{G}q_z + \hat{\lambda}w = \mathbf{m}_3^\top \cdot {}^{F}\tilde{\mathbf{p}} \end{cases} \tag{7} $$

Assuming without loss of generality that ${}^{G}\mathbf{q}$ lies in the x-z plane (i.e., ${}^{G}q_y = 0$), the parameter $\hat{\lambda}$ can be eliminated, yielding:

$$ \begin{cases} {}^{G}q_x = {}^{F}\tilde{\mathbf{p}}^\top \cdot \mathbf{m}_1 - (u\, {}^{F}\tilde{\mathbf{p}}^\top) \cdot \mathbf{m}_2 \\ {}^{G}q_z = {}^{F}\tilde{\mathbf{p}}^\top \cdot \mathbf{m}_3 - (w\, {}^{F}\tilde{\mathbf{p}}^\top) \cdot \mathbf{m}_2 \end{cases} \tag{8} $$

Rearranging into linear form results in:

$$ \begin{bmatrix} {}^{F}\tilde{\mathbf{p}}^\top & -u\, {}^{F}\tilde{\mathbf{p}}^\top & \mathbf{0}^\top \\ \mathbf{0}^\top & -w\, {}^{F}\tilde{\mathbf{p}}^\top & {}^{F}\tilde{\mathbf{p}}^\top \end{bmatrix} \begin{bmatrix} \mathbf{m}_1 \\ \mathbf{m}_2 \\ \mathbf{m}_3 \end{bmatrix} = \begin{bmatrix} {}^{G}q_x \\ {}^{G}q_z \end{bmatrix} \tag{9} $$

Stacking n such linear equations from n corner points produces an overdetermined system:

$$ \mathbf{A}\mathbf{x} = \mathbf{b} \tag{10} $$

where

$$ \mathbf{A} = \begin{bmatrix} {}^{F}\tilde{\mathbf{p}}_1{}^\top & -u_1\, {}^{F}\tilde{\mathbf{p}}_1{}^\top & \mathbf{0}^\top \\ \mathbf{0}^\top & -w_1\, {}^{F}\tilde{\mathbf{p}}_1{}^\top & {}^{F}\tilde{\mathbf{p}}_1{}^\top \\ \vdots & \vdots & \vdots \\ {}^{F}\tilde{\mathbf{p}}_n{}^\top & -u_n\, {}^{F}\tilde{\mathbf{p}}_n{}^\top & \mathbf{0}^\top \\ \mathbf{0}^\top & -w_n\, {}^{F}\tilde{\mathbf{p}}_n{}^\top & {}^{F}\tilde{\mathbf{p}}_n{}^\top \end{bmatrix}, \quad \mathbf{b} = \begin{bmatrix} {}^{G}q_{1,x} \\ {}^{G}q_{1,z} \\ \vdots \\ {}^{G}q_{n,x} \\ {}^{G}q_{n,z} \end{bmatrix} $$

and $\mathbf{x} = [\mathbf{m}_1^\top \;\; \mathbf{m}_2^\top \;\; \mathbf{m}_3^\top]^\top$.

IEEE Robotics and Automation Letters (RA-L) paper, presented at ICRA 2026, Vienna, Austria. Cite as RA-L paper.

Singular Value Decomposition (SVD) is employed to solve this overdetermined system. An analogy can be drawn between this formulation and the Perspective-n-Point problem, given by

$$ {}^{G}\mathbf{q} + \lambda \begin{bmatrix} u \\ 1 \\ w \end{bmatrix} = \mathbf{H} \cdot \begin{bmatrix} {}^{F}p_x \\ {}^{F}p_y \\ {}^{F}p_z \\ 1 \end{bmatrix} \tag{11} $$

where $\mathbf{H}$ represents the homography matrix with eight degrees of freedom due to scale ambiguity. The matrix $\mathbf{M}$ similarly exhibits eight degrees of freedom. At least four corner points ($n \geq 4$) are required to obtain a unique solution for $\mathbf{M}$; hence, the gauge must have no fewer than four intersecting lines. After solving for

$$ \hat{\mathbf{x}} = \begin{bmatrix} \hat{\mathbf{m}}_1^\top & \hat{\mathbf{m}}_2^\top & \hat{\mathbf{m}}_3^\top \end{bmatrix}^\top \tag{12} $$

the matrix $\hat{\mathbf{M}}$ is reconstructed, and $\hat{\mathbf{r}}_2$ is computed via the cross product $\hat{\mathbf{r}}_2 = \hat{\mathbf{r}}_3 \times \hat{\mathbf{r}}_1$. As the elements of $\hat{\mathbf{R}} = [\hat{\mathbf{r}}_1\ \hat{\mathbf{r}}_2\ \hat{\mathbf{r}}_3]$ are estimated independently, orthogonality may not be strictly satisfied. A nearest orthogonal approximation [17] is therefore applied via

$$ \bar{\mathbf{R}} = \mathbf{U}\mathbf{V}^\top \tag{13} $$

where $\mathbf{U}$ and $\mathbf{V}$ are obtained from the SVD of $\hat{\mathbf{R}} = \mathbf{U}\Sigma\mathbf{V}^\top$. The scale ambiguity is resolved by computing the ratio of Frobenius norms, refining the translation as

$$ \bar{\mathbf{t}} = \hat{\lambda}\hat{\mathbf{t}} = \frac{||\bar{\mathbf{R}}||_F}{||\mathbf{R}||_F}\hat{\mathbf{t}}, \tag{14} $$

where $\hat{\mathbf{t}}$ is the initially estimated translation. The closed-form solution for 6-DoF posture estimation is thus given by $(\bar{\mathbf{R}}|\bar{\mathbf{t}})$. To enhance accuracy and robustness, MLE is performed using the closed-form solution as the initial guess. The optimization problem is formulated as

$$ \mathbf{x}(\mathbf{k}^*, \mathbf{t}^*) = \arg\min_{\mathbf{k},\mathbf{t}} \|\mathbf{A}\mathbf{x}(\mathbf{k}, \mathbf{t}) - \mathbf{b}\|_2^2, \tag{15} $$

where the unknown $\mathbf{x}(\mathbf{k}, \mathbf{t}) = \mathrm{vec}((\mathbf{R}(\mathbf{k})|\mathbf{t})^\top)$, with $\mathbf{R}$ parameterized by the unit quaternion $\mathbf{k}$ subject to the constraint $\|\mathbf{k}\|_2 = 1$. The refined estimation is denoted by ${}^{G}_{F}(\mathbf{R}^*|\mathbf{t}^*)$.

D. Corner Detection Pipeline

The mathematical model relies on establishing correspondences between the gauge geometry and n corner points extracted from the laser profiler's cross-sectional scan. The corner detection pipeline proceeds as follows. First, initial corner candidates are identified from the profile polyline using the Ramer-Douglas-Peucker (RDP) algorithm [18]. This algorithm simplifies the polyline by removing redundant data points while preserving critical geometric features. It is assumed that all gauge corners are within the laser profiler's field of view; constraints regarding the gauge geometry and the profiler's measurement range are discussed in detail in Section III-D.

Next, to mitigate the edge noise inherent in laser triangulation, 10% of the data points at both ends of each segment (defined by the initial corner candidates) are discarded. Linear regression is then applied to the remaining points of each segment to obtain refined line equations. Finally, the precise corner coordinates are computed as the intersection points of adjacent fitted lines. This approach is robust to measurement noise and partial occlusions within the segments, ensuring accurate and stable corner extraction for posture estimation.

III. Custom Metallic Gauge Design Guideline

Since the gauge geometry directly imposes the constraints required for solving the 6-DoF posture estimation problem, the estimation quality highly depends on its design. Theoretically, an increased number of corner points in the measured profile imposes more constraints on the linear system $\mathbf{A}\mathbf{x} = \mathbf{b}$, enhancing estimation accuracy and robustness. However, a higher number of corner points necessitates additional gauge planes, increasing fabrication complexity and cost. To balance estimation quality against practical considerations, simulations were conducted to analyze the relationship between the number of corner points and estimation performance. Before presenting the simulation results, the reprojection error metric used to evaluate estimation quality is defined in the following subsection.

A. Reprojection Error

Reprojection error is a widely adopted metric for assessing the accuracy of intrinsic and extrinsic parameter estimation in camera systems. It quantifies the deviation between the actual measured location of a projected 3D point on an image and its predicted location using estimated camera parameters. Formally, in a Perspective-n-Point problem, the reprojection error is defined as the Euclidean distance between the true projection $\mathbf{q}$ of a 3D point $\mathbf{p}$ on the image plane and its estimated projection $\hat{\mathbf{q}}$ obtained through the estimated homography matrix $\hat{\mathbf{H}}$:

$$ d(\mathbf{q}, \hat{\mathbf{q}}) = ||\mathbf{q} - \hat{\mathbf{H}} \cdot \mathbf{p}|| \tag{16} $$

Given the conceptual similarity of the proposed method to the Perspective-n-Point problem, the reprojection error is adopted to evaluate the quality of 6-DoF posture estimation. In the proposed method, it is defined as the distance between the true direction vector $\mathbf{s}$ and the estimated direction vector $\hat{\mathbf{s}}$ of the ridge line $\mathbf{L}$ on which the profile corner point ${}^{F}\mathbf{p}$ lies. The estimated direction vector $\hat{\mathbf{s}} = [\hat{u}\ 1\ \hat{w}]^\top$ is obtained by substituting the estimated 6-DoF posture ${}^{G}_{F}(\bar{\mathbf{R}}|\bar{\mathbf{t}})$ into (4):

$$ d(\mathbf{s}, \hat{\mathbf{s}}) = ||\mathbf{s} - ({}^{G}_{F}(\mathbf{R}^*|\mathbf{t}^*) \cdot {}^{F}\mathbf{p} - {}^{G}\mathbf{q})|| \tag{17} $$

Both $\mathbf{s}$ and $\hat{\mathbf{s}}$ are normalized to have unit y-component for consistency. Simulation studies verified the representativeness of reprojection error for extrinsic parameter errors. The correlation between reprojection errors and 6-DoF posture estimation errors (including both positional and angular components) was assessed using 500 randomly sampled poses. Strong correlations were observed, with coefficients of determination $R^2 = 0.94$ and $R^2 = 0.92$ for positional and angular errors, respectively, confirming the effectiveness of reprojection error as a metric for evaluating 6-DoF posture estimation quality.

IEEE Robotics and Automation Letters (RA-L) paper, presented at ICRA 2026, Vienna, Austria. Cite as RA-L paper.

TABLE I
MEANS AND STANDARD DEVIATIONS OF REPROJECTION ERROR (μm) FOR THE CLOSED-FORM (CF) AND MAXIMUM-LIKELIHOOD-REFINED (CF-OPT) SOLUTIONS ACROSS m RANDOM GAUGES WITH n CORNER POINTS.

	n	m =10	m =50	m =100	m =150
CF	4	-/-	-/-	-/-	-/-
	5	10/10	10/11	9/9	10/10
	7	3/2	4/3	3/2	4/3
	10	3/1	2/1	2/1	2/1
CF-Opt	4	1/*	1/*	1/*	1/*
	5	*/*	*/*	*/*	*/*
	7	*/*	1/*	1/*	1/*
	10	1/*	1/*	1/*	1/*

'-' indicates failure when errors exceed 10^3 μm.
'*' indicates omitted values below 1 μm.

B. Performance with Varying Number of Corner Points

The relationship between estimation quality and the number of corner points in the profile was evaluated through simulation. Simulations were conducted with corner point counts of $n = 4, 5, 7$, and 10. For each n, varying quantities ($m = 10, 50, 100, 150$) of randomly generated gauges with different geometries were used to assess the convergence of performance metrics with respect to gauge geometry. This approach accounts for the influence of geometric variations and ensures result stability. Each randomly generated gauge was tested across 100 random postures to average out posture-dependent variability and isolate the effect of corner count. Gaussian noise with zero mean and a standard deviation of 5 μm, reflecting the laser profiler's repeatability observed in real experiments, was added to simulate realistic measurement conditions. Both the closed-form (CF) solution and the maximum likelihood refined solution (CF-Opt) were evaluated.

As summarized in Table I, the mean and standard deviation of the reprojection error decreased with increasing corner points n, as expected. Across all values of n, the CF-Opt method consistently yielded superior performance, with mean errors at or below 1 μm and standard deviations below 1 μm. The CF solution exhibited elevated errors at $n = 4$, which substantially decreased at $n = 5$. Balancing increased fabrication complexity and associated with additional ridge lines, a corner point of $n = 5$ was determined to provide an optimal trade-off between cost and performance.

C. Robustness of the Gauge Design under Noise

The robustness of the gauge with $n = 5$ corner points was investigated under various levels of measurement noise through simulations. Gaussian noise with zero mean and standard deviations ranging from 0 to 45 μm was applied to the profile data. Based on Table I, which indicates that performance stabilizes beyond $m = 150$ gauge geometries, 150 randomly generated gauges were used for each noise level. Each gauge was tested across 100 randomly selected postures with independently applied noise.

Fig. 3 presents the mean and standard deviation of reprojection errors as functions of noise magnitude. Both metrics exhibit the expected increase with noise level while remaining relatively small, demonstrating the robustness of the proposed method. The CF-Opt solution consistently yields a lower mean and standard deviation of errors compared to the CF solution, confirming the effectiveness of the maximum likelihood refinement. Additionally, the CF-Opt solution exhibits a smoother trend in mean error, indicating enhanced predictability under noise perturbation.

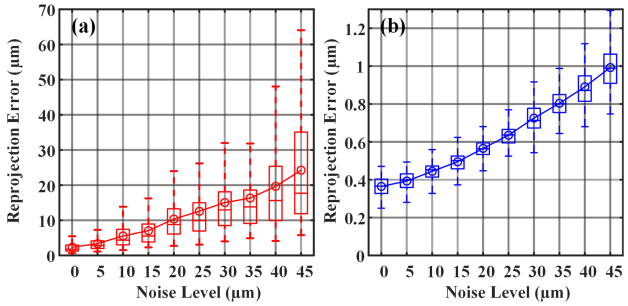

Fig. 3. Reprojection errors versus noise level for (a) closed-form (CF) and (b) maximum likelihood refined (CF-Opt) solutions.

D. Limitations on Gauge Design

The manipulator's permissible range of motion for continuous posture estimation is constrained by the gauge dimensions relative to the fixed measurement range of the laser profiler. First, all gauge corners must remain visible within the laser profiler's field of view during each scan. Consequently, the gauge's physical dimensions along the x- and z-axes of the profile plane must be smaller than the profiler's corresponding measurement limits. While maximizing gauge size in these dimensions yields a profile with more data points—thereby improving the conditioning of linear regression in the corner detection pipeline—minimizing gauge size effectively increases the robot's permissible range of motion. Fig. 4(a) illustrates this relationship: the range of motion along the profiler's x- and z-axes corresponds to the sum of the available margins—defined as the distance between the gauge contour and the boundaries of the profiler's measurement range—on either side of the gauge. Conversely, along the y-axis, the range of motion is determined by the gauge's length; thus, a longer gauge extends the permissible range of motion in that direction. It is important to note that even with a compact gauge, the continuous scanning workspace is smaller than that of typical camera-based systems. Consequently, the proposed method is best suited for small-range applications requiring high feedback rates and stability, such as fine machining tasks.

Second, the gauge geometry imposes constraints on the permissible range of end-effector orientations to avoid self-occlusion. To quantify this relationship, the end-effector orientation is represented by α, defined as the angle between the incident laser ray and the vertical. The gauge geometry is characterized by β, the maximum angle between any gauge plane and the vertical, as illustrated in Fig. 4(b). Since self-occlusion occurs when $\alpha > \beta$, the gauge design must avoid steep planes (which result in a small β) to maximize the permissible orientation range α. The final gauge design adopted in this work (Fig. 1) eliminates small β angles and maximizes

IEEE Robotics and Automation Letters (RA-L) paper, presented at ICRA 2026, Vienna, Austria. Cite as RA-L paper.

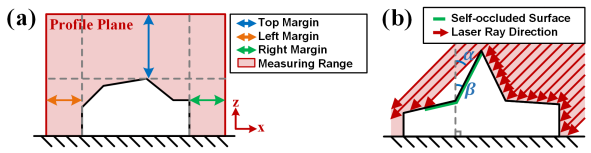

Fig. 4. Design constraints and their impact on the permissible range of motion. (a) The range of motion along the profiler's x- and z-axes is defined by the sum of the available margins on either side of the gauge, which decreases linearly with gauge size. (b) Steep gauge planes must be avoided to prevent self-occlusion at large scanning angles.

dimensions within the experimental workspace constraints to ensure optimal performance.

IV. EXPERIMENTAL VALIDATION

The proposed method was validated through real-world experiments using a gauge with $n = 5$ corner points. The experimental setup is detailed in Sections II-A and II-B.

A. Estimation Quality Evaluation

Estimation quality was assessed under real-world conditions using reprojection error as the primary metric. A total of 250 manipulator postures were randomly generated, and 6-DoF estimation was performed for each. Two solution methods were evaluated to quantify the benefits of refinement: the closed-form solution (CF) and the solution refined via MLE (CF-Opt^a). To address practical fabrication considerations, the refined solution was also tested using a 3D-printed gauge (CF-Opt^b), which offers a more economical and accessible manufacturing alternative to the high-precision metallic gauge. Table II summarizes the mean and standard deviation of the reprojection errors for all 250 postures.

Comparing CF and CF-Opt^a, the former achieved a lower computation time (0.15 ms) but yielded a poorer accuracy and precision. The CF-Opt^a method significantly improved performance, reducing the mean reprojection error to 21.6 μm and the standard deviation to 19.5 μm, confirming the efficacy of the MLE. Comparing gauge types (CF-Opt^a vs. CF-Opt^b), the high-precision metallic gauge (CF-Opt^a) achieved a lower mean reprojection error than the 3D-printed gauge (33.0 μm). This superior accuracy is attributed to the minimized dimensional tolerances of the metallic gauge. However, its smooth surface finish creates challenges for laser triangulation; reduced scattering can increase sensitivity to measurement noise. Conversely, the rougher surface of the 3D-printed gauge enhances diffuse reflection, resulting in a lower standard deviation of 7.1 μm, which indicates greater estimation stability. Consequently, while high-precision gauges are preferable for applications demanding maximum accuracy, 3D-printed gauges offer a cost-effective and highly stable alternative.

B. Speed Comparison with a Camera-based System

The proposed method is designed to bridge the gap between high-cost laser tracker systems and affordable, yet lower-frequency, camera-based solutions. To validate its efficiency,

TABLE II
PERFORMANCE COMPARISON OF CF, CF-OPT^a (HIGH-PRECISION METALLIC GAUGE), AND CF-OPT^b (3D-PRINTED GAUGE).

	CF	CF-Opt^a	CF-Opt^b
Mean (μm)	88.4	21.6	33.0
STD (μm)	85.8	19.5	7.1

^{a} High-precision metallic gauge. ^{b} 3D-printed gauge.

TABLE III
SPEED BENCHMARK WITH TIME COST (ms) OF CAMERA-BASED AND PROPOSED METHODS ACROSS DATA TRANSMISSION (DT), CORNER DETECTION (CD), AND POSTURE COMPUTATION (PC) STAGES.

		Mean / Std	Median	Max	Min
Camera-Based	DT	94.20 / 0.07	94.19	94.38	94.04
	CD	21.64 / 5.43	20.85	33.57	13.51
	PC	0.14 / 0.04	0.12	0.27	0.10
Proposed	DT	6.61 / 0.56	0.65	7.78	5.59
	CD	0.11 / 0.05	0.10	0.20	0.06
	PC	0.26 / 0.14	0.21	0.68	0.12

a comparative speed analysis was conducted between the proposed method and a standard camera-based 6-DoF posture estimation system. The benchmark evaluates three key processing stages: data transmission (DT), corner detection (CD), and posture computation (PC). To ensure a fair comparison, the camera-based system utilized a chessboard target with 3×4 inner corners—the minimum required by the OpenCV library for a unique solution—approximating the 5 corners used in the proposed method. Table III summarizes the statistics from 30 trials for both approaches.

The proposed method demonstrated a significantly faster mean DT time of 6.61 ms compared to 94.20 ms for the camera-based system. This disparity is primarily driven by data size: the 4.80 MB image (2590×1942, 8-bit) is orders of magnitude larger than the 12.8 KB profile data (1×3200, 32-bit). It is worth noting that despite the laser profiler's 1 kHz sampling rate, transmission latency remains non-negligible. Regarding corner detection (CD), the proposed method achieved a mean time of 0.11 ms, whereas the camera-based system required 21.64 ms. This difference results from the computational load of searching a high-resolution image (2590×1942) versus a 1D profile array (1×3200). Posture computation (PC) times were comparable ($<$1 ms) for both methods, as they employ similar algorithms. Statistically, both methods exhibited stable performance with low standard deviations across most metrics. However, the camera-based system showed higher variability in the CD process (std: 5.43 ms). This is attributed to the image processing algorithm's sensitivity to lighting variations, particularly shadows cast by the manipulator in certain postures. Overall, these results confirm that the proposed method offers superior speed and stability for real-time control applications.

C. Real-time Position Control of an Industrial Manipulator

Industrial manipulators frequently execute dynamic trajectories involving rapid motion changes. Due to their kinematic

IEEE Robotics and Automation Letters (RA-L) paper, presented at ICRA 2026, Vienna, Austria. Cite as RA-L paper.

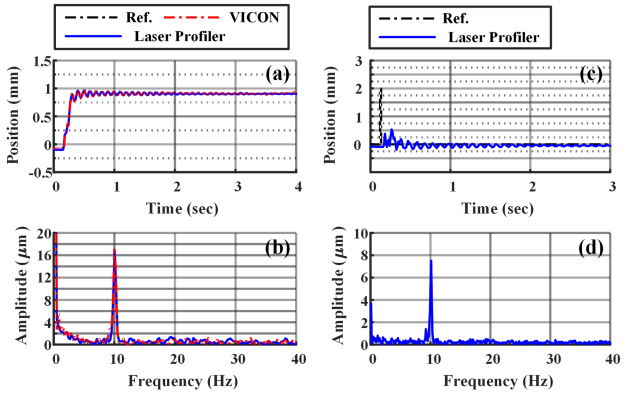

Fig. 5. Open-loop step response measured by VICON and the proposed method: (a) time domain and (b) frequency domain. Impulse response: (c) time domain and (d) frequency domain.

configurations, these manipulators often exhibit low structural stiffness, leading to unexpected dynamic responses such as oscillation during abrupt movements. The high sampling frequency of the proposed method makes it well-suited for real-time closed-loop control to mitigate these behaviors. To validate this capability, a real-time position control experiment was conducted where the performance of open-loop and closed-loop control systems was compared. Both systems utilized the manufacturer's built-in controller operating at 83.3 Hz. The input trajectories consisted of step position commands of the manipulator's end-effector, which simulate sudden motion changes common in industrial applications. In the open-loop configuration, the manipulator relied solely on the built-in controller to track the command without external feedback. In the closed-loop configuration, the 6-DoF posture estimated by the proposed method was fed back into a manually tuned proportional-derivative (PD) controller to compute corrective position commands.

First, the open-loop step responses were measured with the proposed method. To verify measurement accuracy, simultaneous ground-truth data were recorded using a VICON motion capture system at 250 Hz. Fig. 5(a) illustrates the time-domain response, showing post-target oscillations in both the proposed method's measurements and the VICON data, confirming the method's ability to capture manipulator dynamics. The frequency-domain response in Fig. 5(b) reveals a peak at approximately 10 Hz. An impulse response experiment (Fig. 5(c)-(d)) confirmed this as the manipulator's resonance frequency at the target posture. Note that the camera-based system was excluded from these experiments because its sampling frequency falls below the Nyquist rate required to detect these 10 Hz oscillations.

Next, closed-loop step responses using the PD controller were evaluated. The controller gains were tuned using 1 mm step inputs along the orthogonal x, y, and z axes. Subsequently, a composite trajectory moving simultaneously in the $+x$, $+y$, and $+z$ directions was executed. Both 1 mm and 2 mm step inputs were applied to assess controller performance near the operating point. The responses are depicted in Fig. 6. The open-loop responses exhibited 10 Hz oscillations across all axes. The y-axis showed particularly pronounced overshoot, attributed to the high inertia of the manipulator's first joint in that direction. Implementing the PD controller significantly attenuated these oscillations, yielding smoother trajectories. While overshoot was eliminated in the y-axis closed-loop response, settling time remained suboptimal, likely due to nonlinear dynamics uncompensated by the linear PD controller. Quantitative analysis of maximum overshoot (M_p), damping ratio (ζ), and peak frequency magnitude (M_f), summarized in Table IV, confirms that the closed-loop system improved all metrics. Notably, M_p and ζ showed greater improvement for the 1 mm step (for which the controller was tuned), whereas M_f improved more significantly for the 2 mm step, reflecting the suppression of larger oscillation magnitudes.

Further performance gains could be achieved by employing advanced control strategies such as adaptive or fuzzy control to better address nonlinearities. However, as the focus of this work is to demonstrate the real-time capability of the proposed posture estimation method, exploration of such advanced approaches lies beyond the scope of this study.

V. Conclusions and Future Works

This paper presented a real-time 6-DoF posture estimation method for a six-axis industrial manipulator utilizing a 2D laser profiler and a custom-designed metallic gauge. The approach employs a closed-form solution refined via MLE, achieving a substantial improvement in accuracy. By delivering robust and precise measurements at a high sampling frequency, the proposed method bridges the gap between costly laser tracker systems and lower-frequency camera-based systems.

Simulation studies demonstrated that optimal gauge geometry and solution refinement can reduce estimation errors to as low as 1 μm. Real-world validation confirmed that the refined solution consistently outperforms the closed-form approximation, achieving mean reprojection errors of 21.6 μm. Comparative experiments between high-precision metallic and 3D-printed gauges revealed a trade-off: the metallic gauge is preferable for maximum precision, whereas the 3D-printed alternative offers cost-effective fabrication and superior stability (standard deviation of 7.1 μm) due to enhanced surface scattering. Benchmark experiments established the method's advantages over camera-based systems for real-time applications. The proposed system demonstrated significantly lower latencies, with mean processing times of 6.61 ms for data transmission and 0.11 ms for corner detection—substantially faster than the camera-based system. Finally, the practical applicability of the method was verified through a real-time position control loop for a six-axis industrial manipulator. Operating at 83.3 Hz, the system effectively suppressed oscillation in step responses, validating its capability to manage dynamic robotic behaviors.

Future research will focus on implementing nonlinear control strategies to better compensate for manipulator nonlinearities. Additionally, we aim to extend the continuous measurement range of the system and investigate its performance in more complex robotic tasks and unstructured environments.

IEEE Robotics and Automation Letters (RA-L) paper, presented at ICRA 2026, Vienna, Austria. Cite as RA-L paper.

TABLE IV
THE MAXIMUM OVERSHOOT (M_p), DAMPING RATIO (ζ), AND PEAK FREQUENCY MAGNITUDE (M_f) FOR OPEN-LOOP AND CLOSED-LOOP STEP RESPONSES.

		1 mm			2 mm		
		M_p (%)	ζ	M_f (μm)	M_p (%)	ζ	M_f (μm)
x	Open-Loop	5.39 ± 1.34	0.68 ± 0.03	8.30 ± 0.54	4.86 ± 1.22	0.70 ± 0.03	22.52 ± 2.76
	Closed-Loop	2.47 ± 0.55	0.76 ± 0.02	5.14 ± 0.68	3.07 ± 0.59	0.74 ± 0.02	5.46 ± 1.65
	Improvement	54.17%	10.53%	38.07%	36.83%	5.41%	75.75%
y	Open-Loop	65.88 ± 2.27	0.13 ± 0.01	9.69 ± 0.84	39.48 ± 2.69	0.28 ± 0.02	27.26 ± 1.43
	Closed-Loop	20.51 ± 1.72	0.45 ± 0.02	3.58 ± 0.59	1.46 ± 0.96	0.81 ± 0.04	3.49 ± 0.64
	Improvement	68.87%	71.11%	63.05%	96.30%	65.43%	87.20%
z	Open-Loop	13.98 ± 0.91	0.53 ± 0.01	29.86 ± 1.66	8.06 ± 1.03	0.63 ± 0.02	46.64 ± 3.02
	Closed-Loop	2.96 ± 1.05	0.75 ± 0.03	1.90 ± 0.57	1.07 ± 0.28	0.82 ± 0.02	1.7 ± 0.53
	Improvement	78.83%	29.33%	93.64%	86.72%	23.17%	96.36%

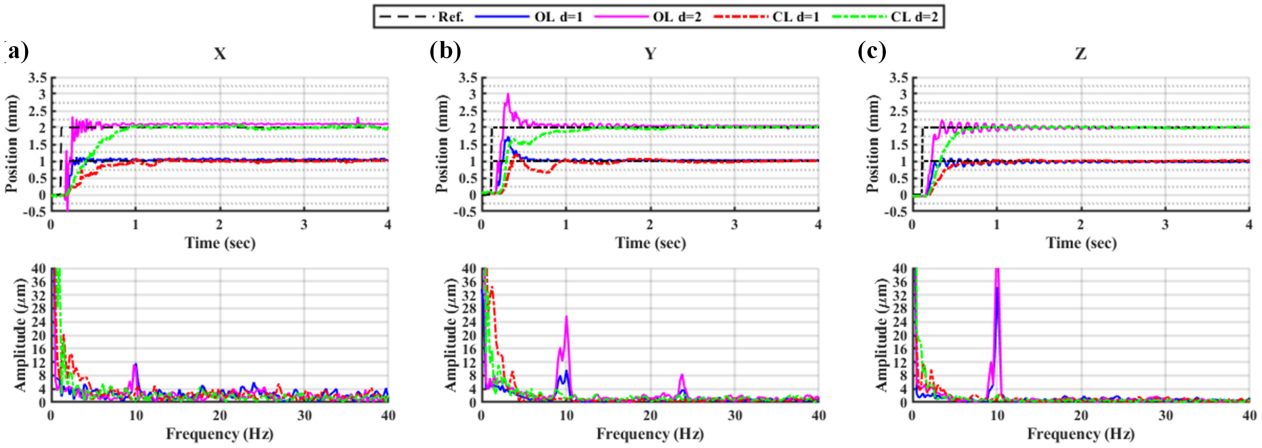

Fig. 6. Step responses of the manipulator using open-loop (OL) and Closed-loop (CL) methods along the (a) x-axis, (b) y-axis, and (c) z-axis.

ACKNOWLEDGMENTS

The authors would like to thank the National Chung-Shan Institute of Science and Technology for their assistance.

REFERENCES

[1] G.-M. Oh and S.-W. Seo, "Fast and robust 6-dof lidar-based localization of an autonomous vehicle against sensor inaccuracy," *IEEE Robotics and Automation Letters*, vol. 9, no. 10, pp. 9095–9102, 2024.

[2] S. Barai and M. Momin, "Outside-in electromagnetic tracking method for augmented and virtual reality 6-degree of freedom head-mounted displays," in *2020 4th International Conference on Intelligent Computing and Control Systems (ICICCS)*, 2020, pp. 467–476.

[3] V. Gaudillière, G. Simon, and M.-O. Berger, "Perspective-2-ellipsoid: Bridging the gap between object detections and 6-dof camera pose," *IEEE Robotics and Automation Letters*, vol. 5, no. 4, pp. 5189–5196, 2020.

[4] L. Clement and J. Kelly, "How to train a cat: Learning canonical appearance transformations for direct visual localization under illumination change," *IEEE Robotics and Automation Letters*, vol. 3, no. 3, pp. 2447–2454, 2018.

[5] J. Lee, K. Kim, and B.-J. You, "Robot arm self-calibration using rgb-d camera," *IEEE Robotics and Automation Letters*, vol. 10, no. 10, pp. 10 258–10 265, 2025.

[6] R. G. Dorsch, G. Häusler, and J. M. Herrmann, "Laser triangulation: fundamental uncertainty in distance measurement," *Appl. Opt.*, vol. 33, no. 7, pp. 1306–1314, Mar 1994.

[7] F. Bologna, M. Tannous, D. Romano, and C. Stefanini, "Automatic welding imperfections detection in a smart factory via 2-d laser scanner," *Journal of manufacturing processes*, vol. 73, pp. 948–960, 2022.

[8] W. Huang and R. Kovacevic, "Development of a real-time laser-based machine vision system to monitor and control welding processes," *The International Journal of Advanced Manufacturing Technology*, vol. 63, pp. 235–248, 2012.

[9] D. Lv, J.-F. Sun, Q. Li, and Q. Wang, "3d pose estimation of ground rigid target based on ladar range image," *Appl. Opt.*, vol. 52, no. 33, pp. 8073–8081, Nov 2013.

[10] T. S. Lembono, F. Suarez-Ruiz, and Q.-C. Pham, "Scalar: Simultaneous calibration of 2-d laser and robot kinematic parameters using planarity and distance constraints," *IEEE Transactions on Automation Science and Engineering*, vol. 16, no. 4, pp. 1971–1979, 2019.

[11] J.-X. Liu, T. Chen, Y.-Y. Tsai, and P.-C. Lin, "A kinematic parameter calibration method of a 6-axis industrial robot using an eye-in-hand 2-d laser profiler," *IEEE Sensors Letters*, vol. 9, no. 7, pp. 1–4, 2025.

[12] L. Huang, Q. Zhang, and A. Asundi, "Camera calibration with active phase target: improvement on feature detection and optimization," *Opt. Lett.*, vol. 38, no. 9, pp. 1446–1448, May 2013.

[13] C. Liu, J. Liu, X. Ao, F. Mo, and R. Yang, "Methods of correction to extrinsic parameters in a stereoscopic vision with the assistance of two known-distance points," *Opt. Lett.*, vol. 49, no. 18, pp. 5304–5307, Sep 2024.

[14] E. Fernández-Moral, J. González-Jiménez, and V. Arévalo, "Extrinsic calibration of 2d laser rangefinders from perpendicular plane observations," *The International Journal of Robotics Research*, vol. 34, no. 11, pp. 1401–1417, 2015.

[15] Q. Zhang and R. Pless, "Extrinsic calibration of a camera and laser range finder (improves camera calibration)," in *2004 IEEE/RSJ International Conference on Intelligent Robots and Systems (IROS)(IEEE Cat. No. 04CH37566)*, vol. 3. IEEE, 2004, pp. 2301–2306.

[16] Z. Zhang, "A flexible new technique for camera calibration," *IEEE Transactions on Pattern Analysis and Machine Intelligence*, vol. 22, no. 11, pp. 1330–1334, 2000.

[17] P. H. Schönemann, "A generalized solution of the orthogonal procrustes problem," *Psychometrika*, vol. 31, no. 1, pp. 1–10, 1966.

[18] D. H. Douglas and T. K. Peucker, "Algorithms for the reduction of the number of points required to represent a digitized line or its caricature," *Cartographica: the international journal for geographic information and geovisualization*, vol. 10, no. 2, pp. 112–122, 1973.